Appl Phys A
DOI 10.1007/s00339-013-7675-6

Applied Physics A
Materials Science & Processing

The growth of nanoscale periodic and dot-like structures on the surface of stainless steel with femtosecond laser pulses in the dry and wet ambient environment

Shazia Bashir · M. Shahid Rafique · Ali Ajami · Wolfgang Husinsky · Umm-i-Kalsoom

Received: 14 December 2012 / Accepted: 16 March 2013

Abstract The present work deals with growth of nanoscale periodic and dot-like structures on the surface of stainless steel (SS) by the irradiation of femtosecond laser pulses. For this purpose Ti: Sapphire femtosecond laser pulses (wavelength of 800 nm, pulse length of 25 fs and pulse repetition rate of 1 kHz) were employed in a dry (air) and liquid confined (deionized water and ethanol) environments. The targets were exposed to 1000 succeeding pulses for various fluences ranging from 50 to 150 mJ cm^{-2}. Nanoscale structures including ripples, and dots were observed by SEM analysis. The growth and dependence of structure-formation on the ambient environment and laser fluence in both central as well as peripheral ablated areas is systematically investigated. The development of nanostructures and nanoripples is correlated with structural analysis carried out by micro Raman spectroscopy.

1 Introduction

Femtosecond lasers have been established to be an excellent and universal tool for micro- and nanostructuring of solid materials. The emergence of self-formed Laser-Induced Periodic Surface Structures (LIPSS) on the surface of metals, semiconductors and insulators is a well known phenomenon and has been investigated by many groups [1–9]. These periodic ripples are attributed to the interference between the incident laser and the surface scattered light field [10, 11]. The advancement of intense femtosecond-pulse laser technology has elucidated some phenomena induced by laser-matter interactions which are completely inaccessible by picoseconds and nanosecond-pulse lasers [12]. The reason behind is that the energy in a femtosecond pulse can be precisely and rapidly deposited in a solid material with fewer thermal effects [1, 3, 4, 7, 9, 13].

The formation of laser-induced periodic surface structures on the stainless steel surface using femtosecond laser pulses is reported by Qi et al. [14]. Under different experimental condition, low-spatial-frequency laser-induced periodic surface structures with a period of 526 nm and high-spatial-frequency laser-induced periodic surface structures with a period of 310 nm were obtained. Hou et al. [15] also investigated the formation of long-periodic (LP) ripples with a period of 530–600 nm and short-periodic (SP) ripples with a period of 260–320 nm on stainless steel after irradiation by 800 nm femtosecond laser pulses. The topographical and chemical effects of femtosecond laser irradiation on industrial steel surfaces are analyzed by Raillard et al. [16]. This work was performed in air and it was observed that the distribution of amorphous and crystalline carbon depends on the distribution of the laser intensity. The increase of the number of pulses leads to the amorphization of the irradiated zones, according to the melt-quenching phenomenon. During nanosecond laser ablation of SS in oxygen environment, in addition to variation in elemental composition, the enhancement in the diffused surface oxygen content is also observed ranging from 19 % to 45 % for various fluences [12].

Due to various cooling and confinement effects and environmental friendly synthesis method laser ablation in liquids

S. Bashir (✉) · M. Shahid Rafique · A. Ajami · W. Husinsky
Institute for Applied Physics, Vienna University of Technology, Vienna, Austria
e-mail: shaziabashir@gcu.edu.pk

S. Bashir
Centre for Advanced Studies in Physics, GC University Lahore, Lahore, Pakistan

M. Shahid Rafique · Umm-i-Kalsoom
Department of Physics, University of Engineering and Technology Lahore, Lahore, Pakistan

Published online: 29 March 2013

has become a powerful emerging technique with substantial scientific, industrial and medical applications [17]. It is more complex due to the effective role by laser-produced plasma of the ambient liquid, enhanced heat conduction, intensified acoustic pressure, increased shock wave duration and additional photo chemical/mechanical effects associated with explosive vaporization [13, 18]. By using this technique the surface modification of the material is possible with debris-free nano and micro structuring [19]. The chemical reactivity of most of the liquids with materials during laser irradiation, results into the formation of oxides, hydro-oxides and metal-alcohols [20, 21]. In the recent work by Barmina et al. [22] it is reported that laser-assisted nanotexturing of W substrates cathodes via ablation in liquid environment has shown an improvement in its thermionic properties.

The present work proposes the mechanism for the emergence of nanoscale ripples and structures on surface of stainless steel induced by femtosecond laser irradiation. The main aim is to explore the effect of the ambient environment (dry or wet) and the laser fluence on the formation of various structures by keeping the number of laser pulses constant. For the analysis of surface morphology SEM analysis has been performed. In the presence of a reactive gas (air) or reactive liquid (deionized water and ethanol), the plume/ambient gas interactions lead to the adsorption of chemically reactive species and cause the structural modification of irradiated surface. For this purpose micro Raman spectroscopy investigations are also performed. The innovative aspect of the present work is the irradiation of SS material by fs laser pulses in both dry (air) and wet (liquid) environments. The influence of ambient environment on the growth of topographical structures and chemical reactivity of material has been explored.

2 Experimental details

Circular disc of commercial grade stainless steel (AISI-304) with diameter of 10 mm and thickness of 5 mm was used as a target. Prior to laser treatments the samples were grinded and polished to a minimum surface roughness of 5 nm. EDS analysis is performed for chemical analysis of an unirradiated sample. All values are with ± 5 % percentage error. During polishing the samples were washed with alcohol and water to eliminate the impurities on the surface and finally ultrasonically cleaned with acetone for 30. The weight percentages of all elements are as follows: C with 9 %, Si with 1 %, Cr with 18 %, Mn with 3 %, Fe with 60 % and Ni with 7 %.

In order to perform irradiation, prepared samples were mounted on the motorized xyz-manipulator (with a few nm resolution) to position the targets precisely for each exposure. The irradiation was performed by using Chirp Pulse Amplification (CPA) Ti: sapphire laser. The system was operated at a repetition rate of 1 kHz with a central wavelength of 800 nm and at pulse duration of 25 fs.

A lens with a focal length of 170 mm was used to focus the laser beam onto the target surface. Beam diameter at the lens is 15 mm. The spot size of the focused beam was calculated to be 12 μm at the focal point. The calculated Rayleigh Length (Z_R) is 0.26 mm. At 5 mm away from the focus point the spot size was 220 μm. The area of focused beam at 5 mm away from the focus comes out to be 1.52×10^{-3} cm^2. Thus the calculated fluences for the average pulse energies (measured by power energy meter before and after passing through the liquids) of 76, 152 and 228 mJ are 50, 100 and 150 mJ/cm^{-2}, respectively.

The exposures were performed by placing the targets 5 mm away from the focus spot in dry (air) and wet (deionized water and ethanol) environment. The laser energy was varied with a polarizer and was monitored by an energy meter (Coherent 210, USA). The SS targets were exposed to 1000 pulses in air (dry), deionized water (wet) and in ethanol (wet) environments for fluence of 50, 100, and 150 mJ cm^{-1}.

The surface topography analysis of the laser irradiated SS was performed with a Scanning Electron Microscope (SEM, FEI-QUANTA 200F, Netherlands).

To explore the structural analysis of ablated targets, micro Raman spectroscopy is performed by a Raman spectrometer Lab Ram HR-800 (Horiba Jobin-Yvon) with a spectral resolution of 3 cm^{-1}. A He-Ne laser is used as an excitation source with 8 mW power, at 632.8 nm. A 20× objective lens is used for laser focusing, resulting in a spot size of ∼20 μm. The spectral data were accumulated at a fixed grating position for one minute and were collected using an air-cooled CCD camera.

3 Results and discussion

3.1 SEM analysis

The assembly of results investigated by SEM comprises three parts namely; the effect of laser fluence on the ablation mechanism in (a) air, (b) deionized water, and (c) ethanol environment

3.1.1 Effect of laser fluence on ablation in air (dry) environment

Figure 1 shows the surface morphologies of central ablated area resulting from the irradiation of the SS target in air by 1000 succeeding laser pulses at fluence of (a) 50 mJ cm^{-2} (b) 100 mJ cm^{-2} and (c) 150 mJ cm^{-2}. Figure 1(a) shows the emergence of Laser Induced Periodic Surface Structures

(LIPSS) with an average periodicity of 400 nm for a fluence of 50 mJ cm^{-2}. In addition to these ripples, within grooves a number of deep-hole structures and micro-size craters are formed causing discontinuity in the appearance of these periodic structures. The formation of nano scale spherical structures on the top of LIPSS can also be seen. Figure 1(b) reveals that increasing fluence results into appearance of more organized and distinct periodic structures with the same periodicity as in Fig. 1(a). Further increase of fluence up to 150 mJ cm^{-2} (c) results in the formation of wider periodic structures with an average periodicity of 500 nm. The clarity of ripples becomes poor. These structures appear to be more polluted by the re-deposited materials from the plume. Such re-deposited material in the form of droplets appear on the upper edges of ripples for a lower fluence of 50 mJ cm^{-2} (Fig. 1a), but cover the whole treated area for the maximum fluence of 150 mJ cm^{-2} as has been exhibited in Fig. 1(c). Their underlying mechanisms could attribute to the local field enhancement of transient surface nanoplasmas, resulting into a nonthermal ablation of metallic targets [1].

Figure 2 exhibits the SEM micrographs of periphery/boundary of the central ablated area of SS irradiated with a fluence of (a) 50 (b) 100 and (c) 150 mJ cm^{-2} for 1000 overlapping pulses. Figure 2(a) reveals nanoripple formation with typical periodicity of 200–250 nm. These ripples are truncated within island-like structures, which are separated by broken boundaries made up of nano-trenches and nanoholes. Figure 2(b) represents appearance of ripples along with random heterogeneities of hundreds of nm in size. These structures are also formed within island-like structures which are separated by distinct boundaries. Figure 2(c) shows that with the increase in the laser fluence to 150 mJ cm^{-2}, the laser-induced surface structures were found to change significantly. It displays the development of semi-organized elevated and uplifting protrusions and feather-like ripple patterns formed within larger island-like structures which are separated by continuous boundaries. Structures are ordered with an average periodicity of 100 nm.

A comparison of SEM analysis of central and peripheral ablated area illustrates that in both cases nanoripples of periodicity smaller than laser wavelength have been observed. However, the periodicity of LIPSS in case of central area is significantly higher than periodicity of grown structures at peripheral ablated area. This is due to the fact the laser fluence due to Gaussian energy distribution is higher at the central portion as compared to that in the outskirts.

Ultrashort laser pulses can induce morphological features on the nanometer scale at the surfaces of irradiated targets. These nanostructures with periodicity much smaller than laser wavelength λ allow the incident E-field to coherently couple with the collective oscillations of free electrons to excite Surface Plasmon Polaritons (SPPs) in the surface layer. The SPP will initiate the nanoscale ablation [23]. Once the ablation is locally induced, self-organized nano periodic structures are created on the surface [24]. These periodic structures are attributed to an inhomogeneous distribution of energy on the surface due to interaction between the incident

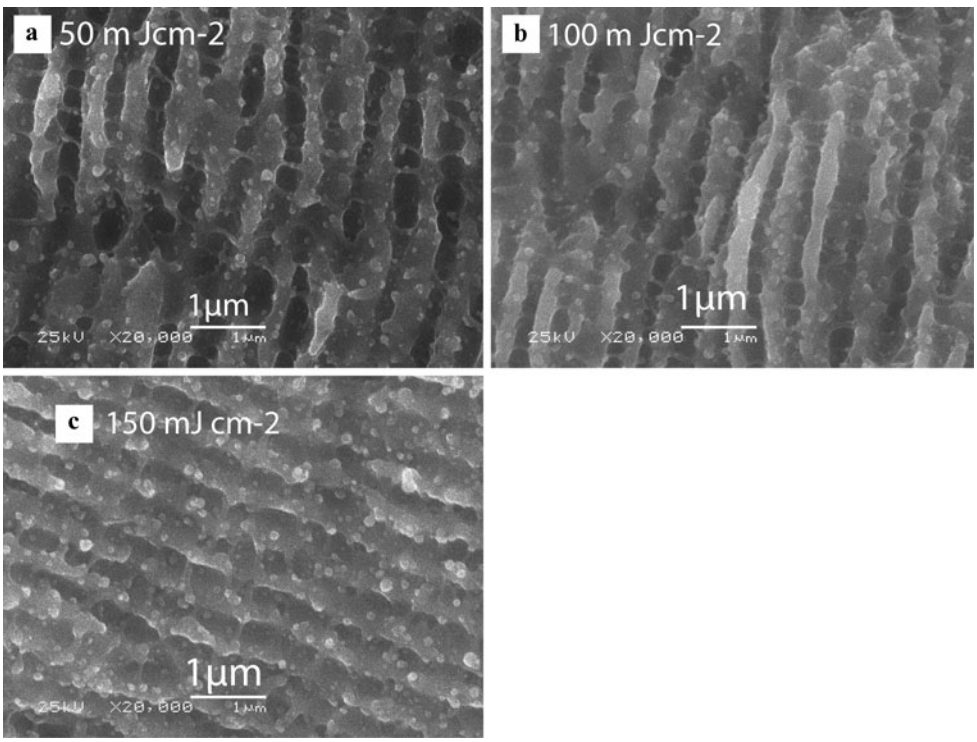

Fig. 1 SEM images revealing the formation of laser induced periodic surface structures at central ablated area resulting from the irradiation of the SS target in air by 1000 succeeding laser pulses for various laser fluences of (**a**) 50 mJ cm^{-2} (**b**) 100 mJ cm^{-2} and (**c**) 150 mJ cm^{-2}

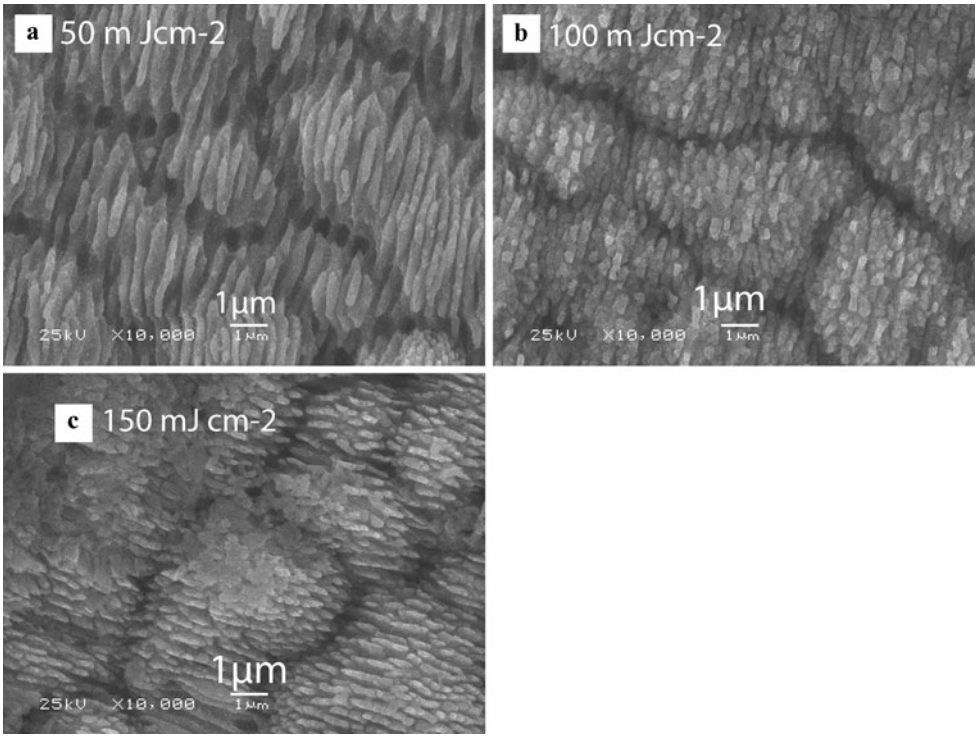

Fig. 2 SEM images revealing the surface morphology of grown nanoripples at peripheral ablated area resulting from the irradiation of the SS target in air by 1000 succeeding laser pulses for various laser fluences of (**a**) 50 mJ cm^{-2} (**b**) 100 mJ cm^{-2} and (**c**) 150 mJ cm^{-2}

light and surface scattered waves or radiation remnant field structures [11, 25]. Thus, in response to spatial modulation of the energy, the modulated modifications on the surface of the materials are formed.

3.1.2 Effect of laser fluence on ablation in deionized water (wet) environment

Figure 3 shows the surface morphologies of central ablated area of irradiated SS in deionized water by 1000 pulses with a fluence of (a) 50, (b) 100 and (c) 150 mJ cm^{-2}. These images demonstrate the formation of more diffused, dispersed and smaller nanoripples than those for air (Fig. 1). The appearance of dots on the top of these nanoripples is also clearly seen. Figure 3(a) shows the appearance of nanoripples with a periodicity of 250–270 nm. Figure 3(b) depicts that increase in laser fluence makes the appearance of dots more distinct with irregular distribution of nanoripples. From Fig. 3(c) it is observed that with the further increase of laser fluence, both the size and the density of dots are significantly enhanced. However, the nanoripples become more distinct and organized at this fluence.

The laser pulses will melt the nanometer scale ripples, because the absorbance in a disturbed/rippled surface becomes higher than that of a smooth surface [26].

Once the ripples are in a molten state, they tend to break up into dots and subsequent laser irradiation cultivates dots into ripples through preferential removal of material around the dots by laser-assisted ablation. Defects and surface texturing in the form LIPSS over multiple length scales can lead to significant reductions in reflectivity and can enhance the absorption of light by the material. A flat surface does not offer further interaction of laser beam with the material. On the other hand, protruding features can reflect and scatter light back onto the surface. Light can effectively become trapped in LIPSS where multiple reflections enhance the coupling into the material [27]. Refraction at the surface of these structures also leads to transmission at oblique angles, effectively increasing the optical path length, enhancing absorption and breaking up of LIPSS into beads [27].

Figure 4 shows various kinds of grown structure at the boundary of the central spot of SS exposed to 1000 laser pulses in deionized water for a fluence of (a) 50, (b) 100, and (c) 150 mJ cm^{-2}. It reveals the formation of high-density regular arrays of nanometer-scale ripples and droplets. Figure 4(a) exhibits that the periodicity of ripples in order of 300–400 nm and the size of droplets is about 100 nm. Figure 4(b) shows that with increasing fluence, dots are locally developed and some of them are joined together across the ridges. The size of these dots is much larger as compared to droplets or dots produced at lower fluence (Fig. 4(a)). Figure 4(c) suggests the growth of micro-scale dot-like structures on the top of ridges. The transformation from nanoscale to micro-scale structures is clearly seen. This figure also illustrates a strong bridging between the pair of dots on neighboring ridges. These dots are separated by the holes within grooves in the underlying periodic structures. The laser-induced ripples alter the reflectivity of the target sur-

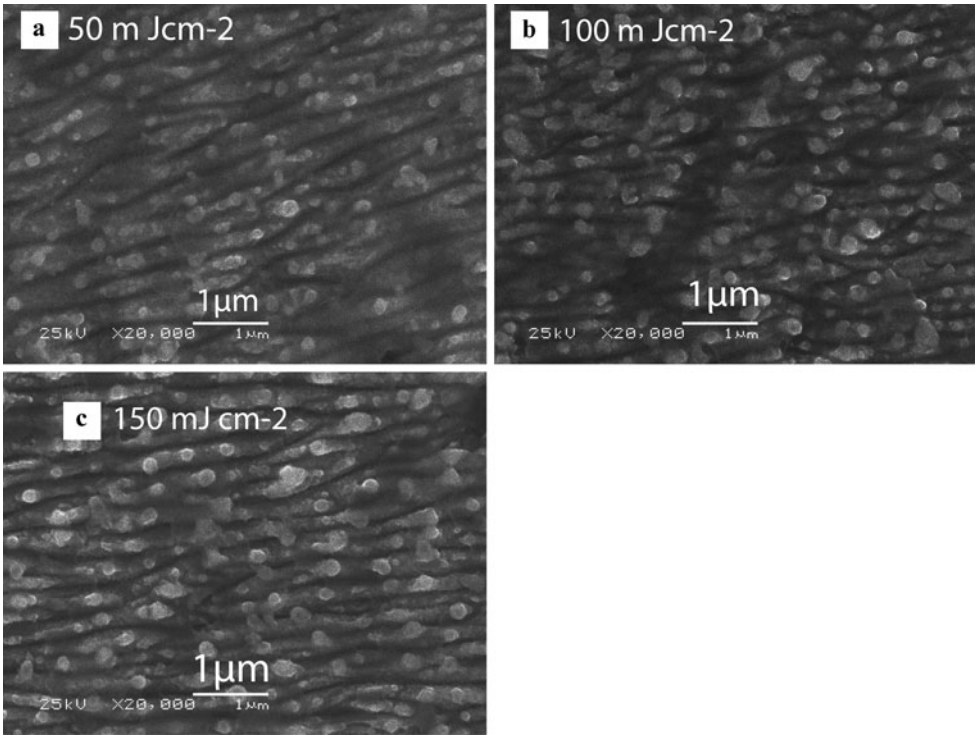

Fig. 3 SEM images revealing the growth of dot-like structures and ripples at central ablated area resulting from the irradiation of the SS target in deionized water by 1000 succeeding laser pulses for various laser fluences of (**a**) 50 mJ cm^{-2} (**b**) 100 mJ cm^{-2} and (**c**) 150 mJ cm^{-2}

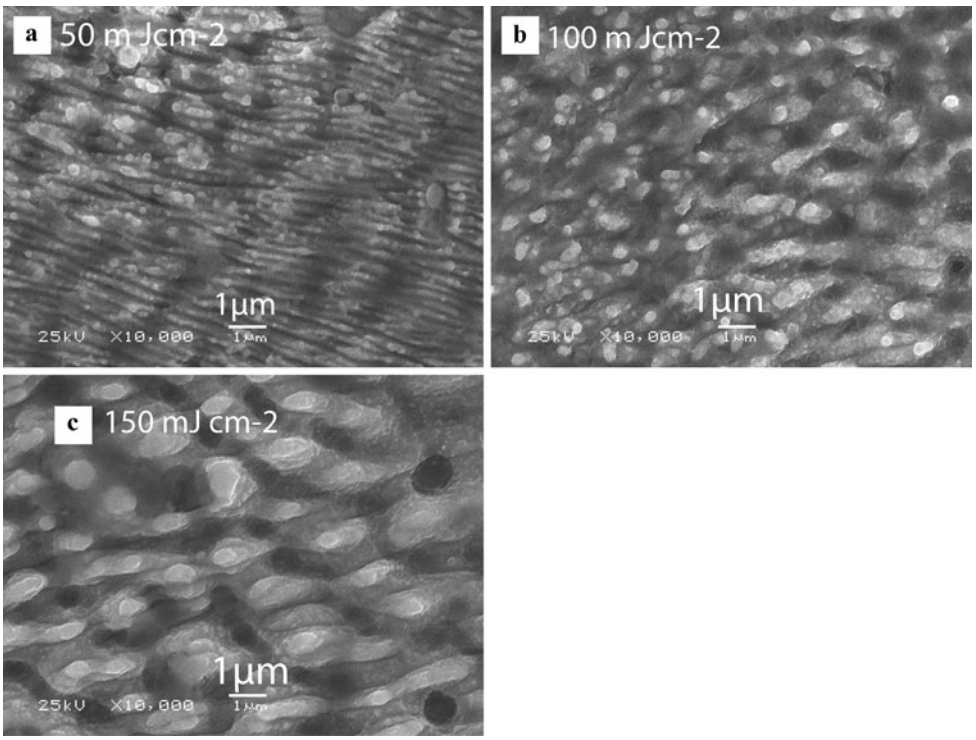

Fig. 4 SEM images revealing various kinds of grown nanostructure at the boundary of the central spot of SS exposed to 1000 laser pulses in deionized water for various laser fluences of (**a**) 50 (**b**) 100 and (**c**) 150 mJ cm^{-2}

face and hence introducing anon-uniform temperature distribution on the target [28, 29]. The non-uniform temperature distribution will then give rise to gradients in the surface tension of the molten material [28]. These gradients are more pronounced in the wet ablation due to enhanced pressure and temperature of the liquid-confined environment and shock wave phenomenon [13, 19]. The enhanced chemical reactivity of the environment [16] also supports the preferential growth of dot-like structures.

3.1.3 Effect of laser fluence on ablation in ethanol (wet) environment

Figure 5 reveals surface morphologies of central ablated area resulting from the irradiation of a SS in ethanol by

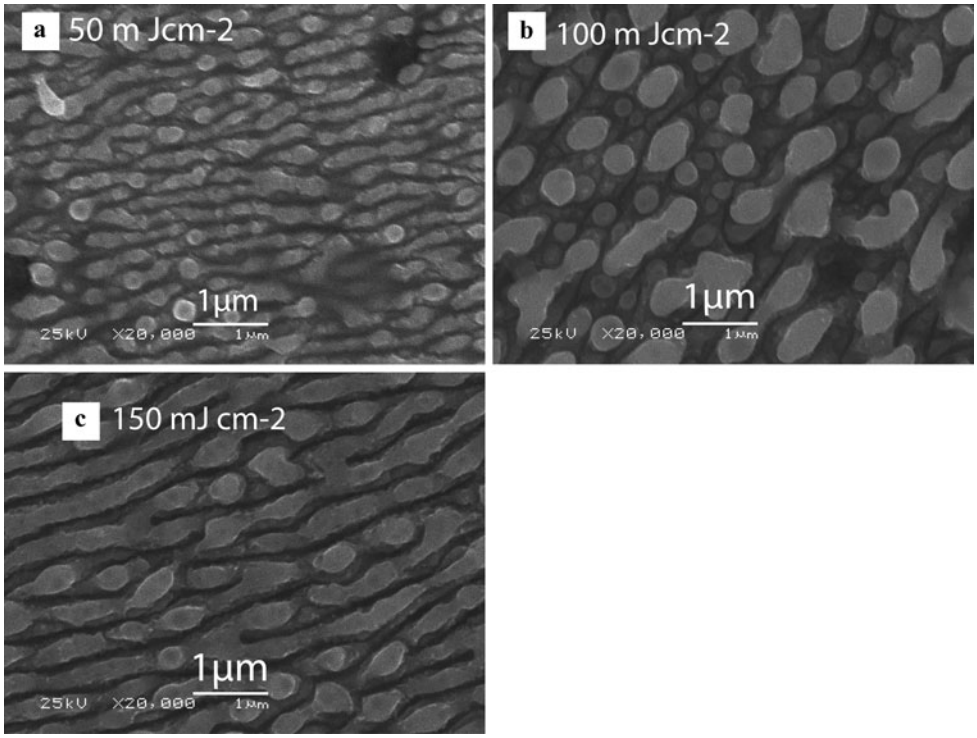

Fig. 5 SEM images revealing the growth of nanostructures at central ablated area resulting from the irradiation of a SS in ethanol by 1000 succeeding pulses of for various laser fluences of (**a**) 50 (**b**) 100 and (**c**) 150 mJ cm^{-2}

1000 succeeding pulses for a fluence of (a) 50, (b) 100 and (c) 150 mJ cm^{-2}. The formation of high-density regular arrays of nano dots and ripples with a typical periodicity of 200–300 nm is clearly seen at 50 mJ cm^{-2} fluence. For an increased fluence of 100 mJ cm^{-2}, it is observed that laser-induced periodic surface structures are destroyed; however, dot-like structures with diameter ranging from 200–600 nm (Fig. 5b) are formed within trenches. Some of these dots have dumbbell-shaped textures in their appearance. The further increase in fluence (Fig. 5c) again results distinct LIPSS with an average periodicity of 400 nm. Some of them are capped with dot-like structures. These images clearly demonstrate that the size, spacing and clarity of structures enhance with increasing fluence.

The surface morphology at the peripheries of ablated SS in ethanol is presented in Fig. 6 at laser fluence of (a) 50, (b) 100, and (c) 150 mJ cm^{-2}. The irregular and circular shaped droplets, droplet coalescence and dot-like structures with hundreds of nanometer size are seen in Fig. 6(a). On the left hand more towards the boundary of ablated area LIPSS are also observed. For higher fluence of 100 mJ cm^{-2}, circular and dumbbell-shaped droplets are seen (Fig. 6b) with enhanced size and regularity. When the fluence is further enhanced to value of 150 mJ cm^{-2} (Fig. 6c) the growth of non-uniform micro sized structures is observed. The coalescence of smaller structures results in formation of larger and unorganized structures at higher fluence.

The chemical interactions of vapors with surrounding atmosphere play a significant role in the formation of the dot-like structures by laser evaporation [30]. The evaporated material during the laser pulse re-condenses on the solidified surface in the form of colloidal structures and clusters with the size depending on the ambient environment. The photon-based ablation of particulates and their subsequent coalescence in a liquid environment is responsible for the growth of dot-like structures [17]. Apparently, the clusters coalesce above the metallic surface and in case of irradiation in liquids they are partially oxidized and also form some content of hydroxides [30].

The appearance of dots can be explained by the involvement of confinement effects of plasma, plasma-caused thermal evaporation of the target as well as erosion effects as a result of the collapse of the cavitation bubble [17, 31].

3.2 Raman spectroscopy analysis

The assembly of results investigated by Raman spectroscopy comprises three parts, namely; the effect of laser fluence on the ablation mechanism in (a) air (b) deionized water and (c) ethanol environment.

1

3.2.1 Effect of laser fluence on ablation in air (dry) environment

Figure 7 shows Raman spectra of SS irradiated with 1000 laser pulses for different fluences of 50, 100 and 150 mJ cm^{-2}

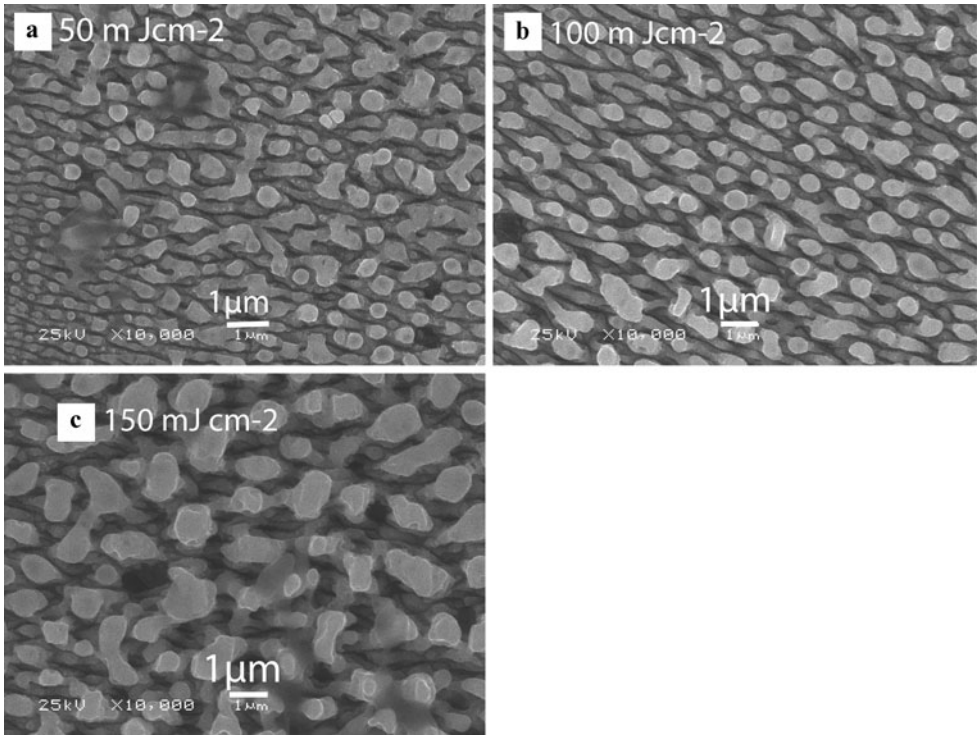

Fig. 6 SEM images revealing the growth of nanostructures at the peripheries of laser ablated SS in ethanol by 1000 succeeding pulses for various laser fluences of (**a**) 50 (**b**) 100 and (**c**) 150 mJ cm^{-2}

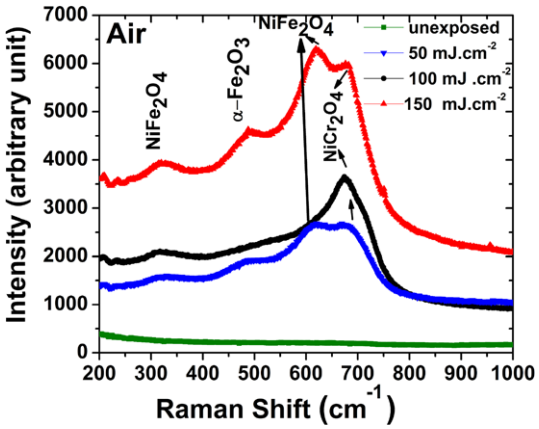

Fig. 7 Raman spectra of laser irradiated SS with 1000 laser pulses for different fluences of 50, 100 and 150 mJ cm^{-2} in air

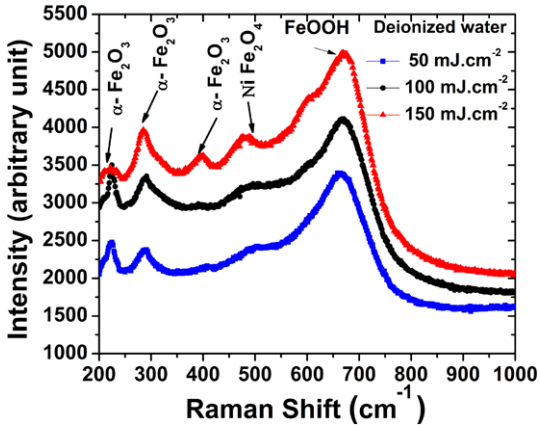

Fig. 8 Raman spectra of laser irradiated SS with 1000 laser pulses for different fluences of 50, 100 and 150 mJ cm^{-2} in deionized water

in air. There is no Raman signal observed for an unexposed target. Raman modes have developed from laser-induced decomposition and formation of oxides on the metal surface after irradiation. For all fluences five major peaks have emerged at approximately 222, 322, 492, 662, and 675 cm^{-1}, corresponding to α-Fe_2O_3, $NiFe_2O_4$, α-Fe_2O_3, $NiFe_2O_4$, and $NiCr_2O_4$ [32–34]. For the lowest fluence the intensity of these peaks is smaller. With the increase of fluence more intense peaks are observed. This represents the enhancement of various kinds of (Fe, NiFe and NiCr) oxide contents in the irradiated alloy.

3.2.2 *Effect of laser fluence on ablation in de-ionised water (wet) environment*

Figure 8 shows Raman spectra of SS irradiated with 1000 laser pulses for different fluences of 50, 100 and 150 mJ cm^{-2} in deionized water.

Five major peaks are identified at 222, 287, 384, 488, 668 cm^{-1}. These peaks correspond to α-Fe_2O_3, α-Fe_2O_3, α-Fe_2O_3, $NiFe_2O_4$ and FeOOH [32–34]. The increase in the peak intensity is observed for increasing fluence except for the peak emerging at 222 cm^{-1}, which corresponds to α-Fe_2O_3. It is observed that in case of deionized water in addition to oxides, hydroxides are also formed.

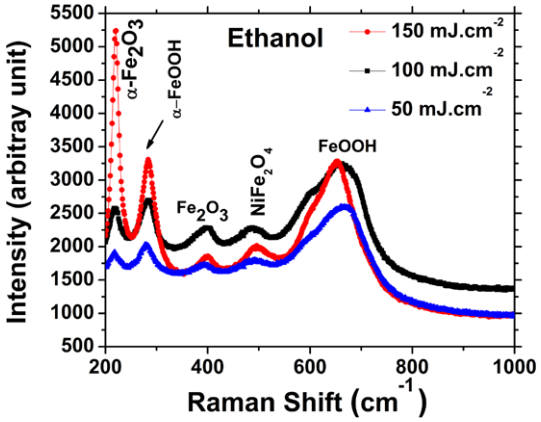

Fig. 9 Raman spectra of laser irradiated SS with 1000 laser pulses for different fluences of 50, 100 and 150 mJ cm^{-2} in ethanol

3.2.3 Effect of laser fluence on ablation in ethanol (wet) environment

Figure 9 shows Raman spectra of stainless steel after multipulse (1000) irradiation for different fluences of 50, 100 and 150 mJ cm^{-2} in ethanol. Five major peaks have been identified at 219, 299, 390, 492 cm^{-1}, and 668 cm^{-1}. These peaks correspond to α-Fe_2O_3, α-FeOOH, Fe_2O_3 $NiFe_2O_4$, and FeOOH [32–34].

With the increase of fluence the intensity of almost all bands increases, which indicates more oxidation and hydroxide formation on the surface and gives rise to a species with characteristic vibrational frequency [33]. The peak appearing at 492 cm^{-1} shifts towards lower position and represents the formation of the new band α-FeOOH at higher fluences [33]. In this case both hydroxides and oxides are formed, but the content of hydroxide has been enhanced as compared to deionized. The same compounds identified by Raman peaks are in different positions. Stresses induced by the laser are responsible for the shifting of these peaks (which is within a certain range).

4 Conclusions

The growth of nanostructure and nanoripples on the surface of SS with femtosecond laser pulses in dry and wet ambient environment has been addressed. It is revealed that the average size, depth, periodicity, and density of femtosecond laser-induced nanostructure features can be controlled by varying both the laser fluence and the ambient environment. The structures that are grown on peripheral ablated areas are of smaller size than grown structures at central ablated areas. In case of dry ablation, only ripples are grown, whereas for wet ablation both nanoscale ripples and dot-like structures are grown. The structural and compositional heterogeneities, the collapse of a plasma-induced cavitation bubble, surface clusters, heir coalescence and secondary phases (oxides and hydroxides) are responsible for the formation of dot like structures in case of wet ablation. Therefore the ambient liquid plasma (formation of oxides and hydroxides) plays a significant role in the surface and structural modification of metallic alloys during laser ablation.

References

1. S. Sakabe, M. Hashida, S. Tokita, S. Namba, K. Okamuro, Mechanism for self-formation of periodic grating structures on a metal surface by a femtosecond laser pulse. Phys. Rev. B **79**(3), 033409 (2009)
2. A.Y. Vorobyev, C. Guo, Spectral and polarization responses of femtosecond laser-induced periodic surface structures on metals. J. Appl. Phys. **103**, 043513 (2008)
3. X.C. Wang, G.C. Lim, F.L. Ng, W. Liu, S.J. Chua, Femtosecond pulsed laser-induced periodic surface structures on GaN/sapphire. Appl. Surf. Sci. **252**, 1492–1497 (2005)
4. Y. Shimotsuma, P.G. Kazansky, J. Qiu, K. Hirao, Self-organized nanogratings in glass irradiated by ultrashort light pulses. Phys. Rev. Lett. **91**, 247405 (2003)
5. S. Bashir, M. Shahid Rafique, W. Husinsky, Femtosecond laser-induced subwavelength ripples on Al, Si, CaF2 and CR-39. Nucl. Instrum. Methods B **275**, 1–6 (2012)
6. D. Dufft, A. Rosenfeld, S.K. Das, R. Grunwald, J. Bonse, Femtosecond laser-induced periodic surface structures revisited: a comparative study on ZnO. J. Appl. Phys. **105**, 034908 (2009)
7. J. Reif, O. Varlamova, F. Costache, Femtosecond laser induced nanostructure formation: self-organization control parameters. Appl. Phys. A **92**, 1019–1024 (2008)
8. M. Huang, F. Zhao, Y. Cheng, N. Xu, Z. Xu, Mechanisms of ultrafast laser-induced deep-subwavelength gratings on graphite and diamond. Phys. Rev. B **79**, 125436 (2009)
9. T. Tomita, K. Kinoshita, S. Matsuo, S. Hashimoto, Effect of surface roughening on femtosecond laser-induced ripple structures. Appl. Phys. Lett. **90**, 153115 (2007)
10. M. Birnbaum, Semiconductor surface damage produced by Ruby lasers. J. Appl. Phys. **36**, 3688–3689 (1965)
11. J.F. Young, J.S. Preston, H.M. Van Driel, J.E. Sipe, Laser-induced periodic surface structure. II. Experiments on Ge, Si, Al, and brass. Phys. Rev. B **27**, 1155–1172 (1983)
12. Umm-i-Kalsoom, S. Bashir, N. Ali, M. Akram, K. Mahmood, R. Ahmad, Effect of ambient environment on excimer laser induced micro and nano-structuring of stainless steel. Appl. Surf. Sci. **261**, 101–109 (2012)
13. H.W. Kang, H. Lee, A.J. Welch, Laser ablation in a liquid-confined environment using a nanosecond laser. J. Appl. Phys. **103**, 083101 (2008)
14. L. Qi, K. Nishii, Y. Namba, Regular subwavelength surface structures induced by femtosecond laser pulses on stainless steel. Opt. Lett. **34**, 1846–1848 (2009)
15. S. Hou, Y. Huo, P. Xiong, Y. Zhang, S. Zhang, T. Jia, Z. Sun, J. Qiu, Z. Xu, Formation of long- and short-periodic nanoripples on stainless steel irradiated by femtosecond laser pulses. J. Phys. D, Appl. Phys. **44**, 505401 (2011)
16. B. Raillard, L. Gouton, E. Ramos-Moore, S. Grandthyll, F. Müller, F. Mücklich, Ablation effects of femtosecond laser functionalization on steel surfaces. Surf. Coat. Technol. **207**, 102–109 (2012)
17. A.V. Kabashin, M. Meunier, Femtosecond laser ablation in aqueous solutions: a novel method to synthesize non-toxic metal colloids with controllable size. J. Phys. Conf. Ser. **59**, 354–359 (2007)

18. V. Amendola, M. Meneghetti, Laser ablation synthesis in solution and size manipulation of noble metal nanoparticles. Phys. Chem. Chem. Phys. **11**, 3805–3821 (2009)
19. S. Bashir, H. Vaheed, K. Mahmood, Nanosecond pulsed laser ablation of brass in a dry and liquid-confined environment. Appl. Phys. A **110**, 389–395 (2013)
20. H.W. Kang, H. Lee, A.J. Welch, Laser ablation in a liquid-confined environment using a nanosecond laser pulse. J. Appl. Phys. **103**, 083101 (2008)
21. S.C. Singh, R.K. Swarnkar, R. Gopal, J. Nanopart. Res. **11**, 1831–1838 (2009)
22. E.V. Barmina, A.A. Serkov, E. Stratakis, C. Fotakis, V.N. Stolyarov, I.N. Stolyarov, G.A. Shafeev, Laser-assisted nano-texturing of W substrates cathodes via ablation in liquid environment. Appl. Phys. A **106**, 1–4 (2012)
23. G. Miyaji, K. Miyazaki, Nanoscale ablation on patterned diamondlike carbon film with femtosecond laser pulses. Appl. Phys. Lett. **91**, 123102 (2007)
24. G. Miyaji, K. Miyazaki, Origin of periodicity in nanostructuring on thin film surfaces ablated with femtosecond laser pulses. Opt. Express **16**, 16265–16271 (2008)
25. H.M. Van Driel, J.E. Sipe, J.F. Young, Laser-induced periodic surface structure on solids: a universal phenomenon. Phys. Rev. Lett. **49**, 1955–1958 (1982)
26. S. Bashir, M. Shahid Rafique, W. Husinsky, A. Hobro, B. Lendl, Atomic force microscopy and Raman scattering studies of femtosecond laser-induced nanohillocks on CR-39. Nucl. Instrum. Methods B **267**, 3606–3610 (2009)
27. P. Campbell, Enhancement of light absorption from randomizing and geometric textures. J. Opt. Soc. Am. B **10**, 2410–2415 (1993)
28. M.S. Trtica, B.M. Gakovic, B.B. Radak, D. Batani, T. Desai, M. Bussoli, Periodic surface structures on crystalline silicon created by 532 nm picosecond Nd: YAG laser pulses. Appl. Surf. Sci. **254**, 1377–1381 (2007)
29. G. Miyaji, W. Kobayashi, K. MIyazaki, Reflectivity change in nanoscale modification of DLC film with femtosecond laser pulses. J. Laser Micro Nanoeng. **2**, 146–151 (2007)
30. C. Burda, X. Chen, R. Nayanan, M.A. Elsayed, Chemistry and properties of nanocrystals of different shapes. Chem. Rev. **105**, 1025–1102 (2005)
31. A. Vogel, J. Noack, K. Nahen, D. Theisen, S. Busch, U. Parlitz, D.X. Hammer, G.D. Noojin, B.A. Rockwell, R. Birngruber, Energy balance of optical breakdown in water at nanosecond to femtosecond time scales. Appl. Phys. B **68**, 27 (1999)
32. L.J. Oblonsky, T.M. Devine, A surface enhanced Raman spectroscopic study of the passive films formed in borate buffer on iron, nickel, chromium and stainless steel. Corros. Sci. **37**, 17–41 (1995)
33. M.G.S. Ferreira, T. Moura e Silva, A. Catarino, M. Pankuch, C.A. Melendres, Electrochemical and laser Raman spectroscopy studies of stainless steel in 0.15 M NaCl solution. J. Electrochem. Soc. **139**, 3146–3151 (1992)
34. B.D. Hosterman, Raman spectroscopic study of solid solution spinel oxides. Physics Ph.D. thesis (2011)